Itinerant magnetism and electronic properties of $FeGe_2$

1991 J. Phys.: Condens. Matter 3 7199

(http://iopscience.iop.org/0953-8984/3/37/012)

J. Phys.: Condens. Matter 3 (1991) 7199–7208. Printed in the UK

Itinerant magnetism and electronic properties of $FeGe_2$

G E Grechnev†, J Kübler‡ and I V Svechkarev†

†Physico-Technical Institute of Low Temperatures, Khar'kov, Ukraine, USSR
‡Institut für Festkörperphysik, Technische Hochschule, D-6100 Darmstadt, Federal Republic of Germany

Received 26 April 1991

Abstract. The electronic and magnetic structure of tetragonal $FeGe_2$ is determined using the local spin-density functional approximation and the ASW method to solve the band-structure problem self-consistently. The calculations reveal that the collinear antiferromagnetic structure—in contrast to a non-collinear one—has the lowest total energy and seems the most preferable candidate for the low-temperature ground-state phase of $FeGe_2$ in agreement with recent neutron diffraction experiments. The calculated Fermi surface cross-sections and cyclotron masses are in good agreement with the DHVA experimental data. From the DHVA and heat capacity data together with the results of band-structure calculations the average value of the electron–phonon interaction constant $\lambda \cong 0.5$ has been deduced for $FeGe_2$. For the alternative non-collinear model we obtained a higher value of the total energy and poor agreement with the DHVA experiment.

1. Introduction

The transition metal compounds with germanium and tin having the tetragonal $CuAl_2$-type structure show many unusual magnetic, electrical and thermal properties [1–11]. For the $FeGe_2$ compounds, the magnetic susceptibility [5], magnetostriction [9], specific heat [5, 10] and neutron scattering [10] exhibit two features at temperatures $T_1 \simeq 263$ and $T_2 \simeq 289$ K. The temperature T_2 corresponds to a transition from the paramagnetic phase to a spiral spin structure propagating along the cell edges in the basal plane [10]. Except for unconfirmed claims of ferromagnetism [12], there are two contradicting models for the low-temperature ($T < T_1$) antiferromagnetic structure of $FeGe_2$. A powder neutron diffraction study [1,3] gives a magnetic structure having a collinear sublattice of moments on the Fe atoms in the basal plane. But neutron diffraction on single crystals [2, 11] suggests a non-collinear structure with an angle between the Fe moments in neighbouring planes of 72° [2] or 28° [11]. Arguing against the non-collinear model Corliss *et al* [10] declared some single-crystal neutron reflections as spurious, produced by double-Bragg nuclear scattering. Nevertheless the problem concerning the low-temperature magnetic structure of $FeGe_2$ is still unresolved and requires theoretical consideration including first-principles calculations of the electronic and magnetic ground-state properties.

Such electronic structure calculations are also required when de Haas–van Alphen (DHVA) measurements exist [6,8]. These experimental results can shed light on the low-temperature magnetic structure provided some reliable model of the electronic structure is available. The band structure of $FeGe_2$ was calculated [13] for the

0953-8984/91/377199+10$03.50

paramagnetic phase using the self-consistent LMTO method [14, 15]. It was established that a sharp peak is present in the electronic density of states at the Fermi level as well as distinct p–d hybridization in the conduction band. This paramagnetic band structure is in qualitative agreement with the room temperature experimental x-ray spectrum data [7] but it cannot explain the low-temperature properties including antiferromagnetism and the DHVA data.

Recently the local approximation to spin-density-functional (SDF) theory has been formulated [16–18] such that non-collinear, itinerant magnetic systems can now be treated. Here, this implementation of SDF theory is applied to $FeGe_2$ in order to solve the problem of finding the correct low-temperature magnetic structure and to explain the DHVA results.

2. Theoretical background

The solution of the self-consistent-field problem that is posed by the spin-density-functional theory [19] is achieved by using the augmented spherical wave (ASW) method [20]. The effective single-particle Hamiltonian now becomes a two-component quantity of the form

$$H = -\nabla^2 1 + \sum_n \left[v_0(|\boldsymbol{r} - \boldsymbol{R}_n|)1 + \Delta v(|\boldsymbol{r} - \boldsymbol{R}_n|) U_n^+ \sigma_z U_n \right] \theta_n(|\boldsymbol{r} - \boldsymbol{R}_n|) \tag{1}$$

where 1 is the unit 2×2 matrix, the sum on n extends over all lattice sites defined by set of vectors $\{\boldsymbol{R}_n\}$, $v_0(\boldsymbol{r})$ is the spin-independent part of the effective single-particle potential whereas $\Delta v(\boldsymbol{r})$ is the spin-dependent part, $\theta_n(|\boldsymbol{r}|)$ is the step function that equals unity for $|\boldsymbol{r}|$ smaller than the atomic sphere radius, S_n, at the site n and zero otherwise, and σ_z is a Pauli spin matrix. The potentials v_0 and Δv are unambiguously given by functional derivatives in the SDF approximation [19] and U_n is the standard spin-$\frac{1}{2}$ rotation matrix that determines the transformation between the global spin-coordinate system and the local one, the latter having spin-quantization axes parallel to the magnetic-moment directions; in other words, polar angles θ_n and φ_n define the direction of magnetization in the nth atomic sphere with respect to some global axis.

We next construct a Bloch spinor function writing

$$\psi_{\boldsymbol{k}}(\boldsymbol{r}) = \sum_{L\sigma\nu} c_{L\sigma\nu}(\boldsymbol{k}) \Phi_{L\sigma\nu\boldsymbol{k}}(\boldsymbol{r}) \tag{2}$$

where L denotes both angular momentum quantum numbers ℓ and m, $\sigma = 1, 2$ denotes two possible bispinors and ν sums over the basis vectors in the unit cell. The spinors Φ are constructed using augmented spherical waves [20] as described before by Sticht *et al* [18]. Assuming, for simplicity, the atomic sphere approximation and, furthermore, that $\boldsymbol{r}$ is inside and centred in the νth sphere, we can write

$$\Phi_{L\sigma\mu\boldsymbol{k}}(\boldsymbol{r}) = \delta_{\nu\mu} \tilde{H}_{L\sigma\nu}(\boldsymbol{r}) + \sum_{L'\sigma'} G^{\nu\mu}_{L\sigma L'\sigma'}(\boldsymbol{k}) \tilde{J}_{L'\sigma'\nu}(\boldsymbol{r}) \tag{3}$$

where $\tilde{H}_{L\sigma\nu}(\boldsymbol{r})$ and $\tilde{J}_{L\sigma\nu}(\boldsymbol{r})$ are augmented Hankel spinor functions and Bessel spinor functions, respectively, centred at the νth atomic sphere, being zero outside,

and the quantity $G^{\nu\mu}_{L\sigma L'\sigma'}(k)$ is connected with the KKR structure constant, $B^{\nu\mu}_{LL'}(k)$, by

$$G^{\nu\mu}_{L\sigma L'\sigma'}(k) = B^{\nu\mu}_{LL'}(k)U_\mu U^+_\nu \tag{4}$$

where U_μ is again the spin-$\frac{1}{2}$ rotation matrix, and where we defined the structure constants to be zero for $\nu = \mu$.

Using (2) and (3) one can formulate the Rayleigh–Ritz variational problem for the coefficients $c_{L\sigma\nu}(k)$ and whence the charge and spin densities. In general, the Hamiltonian matrix is not spin-diagonal [18], and the orientation of the magnetic moments in a given atomic sphere, ν, with respect to a global quantization axis is contained in the spin-$\frac{1}{2}$ rotation matrices U_ν in a standard way. Finally, Sticht *et al* [18] described how the local spin-diagonal frame of reference that is needed to carry out the calculations can always be found.

3. Band structure and itinerant magnetism of $FeGe_2$

The compound $FeGe_2$ has the tetragonal structure C16, space group D^{18}_{4h}. It has four formula units in the unit cell and is illustrated in figure 1. The lattice parameters are given in [10] as $a = 11.1286$ au and $c/a = 0.838$. These values presumably correspond to $T \cong 80$ K. We used this value of c/a for our calculations rather than trying to obtain it from the minimum of the total energy, E_{tot}. Concerning the lattice constant a, we varied it in the vicinity of the experimental value looking for the corresponding minimum of E_{tot}.

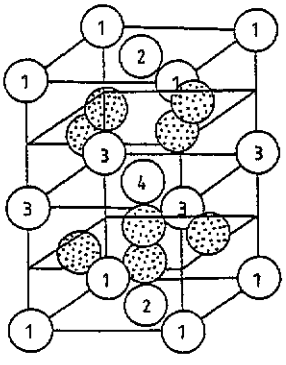

Figure 1. Collinear magnetic-moment arrangements of Fe atoms in the $FeGe_2$ unit cell. Ge atoms are represented by dotted circles and Fe by open circles. For iron atoms 1, 2, 3 and 4 in the unit cell magnetic moments correspond to: (A) ferromagnetic structure $S_1 = S_2 = S_3 = S_4$, (B) antiferromagnetic structure $S_1 = -S_4 = -S_2 = S_3$, (C) BCC antiferromagnetic structure $S_1 = S_4 = -S_2 = -S_3$, (D) antiferromagnetic structure $S_1 = -S_4 = S_2 = -S_3$.

The calculation of the paramagnetic band structure for $FeGe_2$ seems a reasonable starting point in order to compare it with the previous LMTO results [13–15]. Our calculations confirmed the presence of the sharp peak in the density of states at the Fermi level for paramagnetic $FeGe_2$. The dependence of the total energy on the lattice constant a is given in table 1. For trial values a from this table we studied

Table 1. Total energy for a set of lattice constants, a, and assumed non-magnetic, ferromagnetic and antiferromagnetic states.

a (au)	E_{tot} + 21 637 000.0 mRyd (per 2 molecules, Fe_2Ge_4)		
	Paramagnetic	Ferromagnetic	Antiferromagnetic
10.9	−87.366	− 99.682	−104.123
10.942	−87.799*		
10.968		−100.705*	−105.458
10.984			−105.614*
11.0	−86.982	−100.501	−105.464
11.06			−103.879
11.1	−81.391		
11.1286 (77 K)	−80.046	− 95.524	− 99.132
11.146 (300 K)	−78.470	− 93.920	
11.164		− 93.075	− 98.061

* Corresponding minimum of the total energy.

the behaviour of the paramagnetic E_{tot} under variations of the atomic radii ratio R_{Ge}/R_{Fe}, and found it to minimize E_{tot} for $R_{Ge}/R_{Fe} = 1.095$. This value was kept fixed for all other spin-polarized calculations.

To enumerate the possible magnetic structures of $FeGe_2$ we refer to [4], where all collinear configurations were considered (see figure 1 there) and [2, 11] for non-collinear models. For convenience we will consider magnetic moments lying in the basal planes in agreement with the neutron diffraction data [1–4, 10, 11]. Indeed, in the present formalism the sublattice of magnetic moments (the global quantization axis) is not coupled with the crystal axes because we omitted the spin–orbit coupling.

For the ferromagnetic configuration described in the caption to figure 1 we obtain the equilibrium magnetic moment as 1.16 μ_B, and lower values of E_{tot} in comparison with the paramagnetic one (see table 1). But for two possible antiferromagnetic configurations, namely C and D in figure 1, the self-consistent spin-polarized calculations converged to the paramagnetic case with almost zero magnetic moment. This gives us direct evidence of the magnetic instability for these configurations, but this has not yet been experimentally observed [10].

The antiferromagnetic configuration B (figure 1) seems the most preferable of all collinear cases judging from the E_{tot} values listed in table 1. The magnetic moment of Fe in this configuration is calculated to be 1.23 $\mu_B \mp 3\%$ in fair agreement with the experimental value 1.2 μ_B [10, 11]. The uncertainty, $\mp$ 3%, depends on the value of the lattice parameter a that is chosen from the experimental and the theoretical values. As can be seen from table 1, the difference between the first-principles and experimental values of a is about 1%. The calculated band structure and the density of states for this collinear antiferromagnetic configuration are shown in figure 2 and figure 3. The density of states at the Fermi level is considerably reduced in comparison with the paramagnetic case. Indeed a narrow dip can be seen in figure 3 at E_F.

For the non-collinear configurations the ground-state properties were calculated for a set of angles 2φ between the Fe moments in neighbouring basal planes. As can be seen in table 2, the total energy as well as the density of states at the Fermi level increase when the moments turn away from the collinear antiferromagnetic arrangement B in figure 1. The latter has the lowest total energy and seems the most

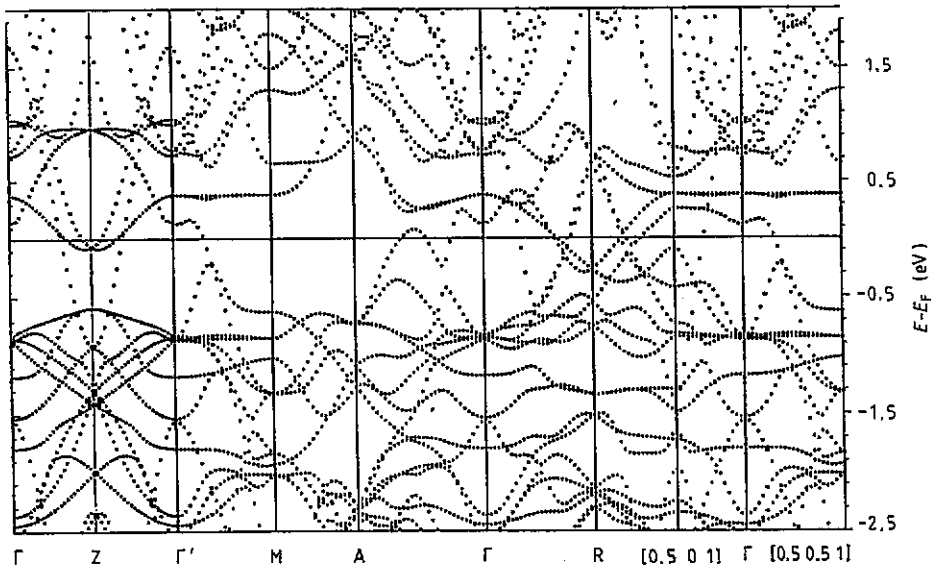

Figure 2. Band structure of collinear antiferromagnetic $FeGe_2$.

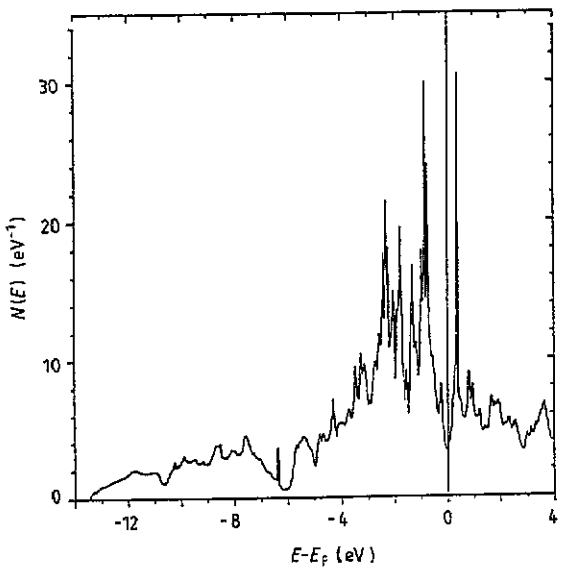

Figure 3. Density of states of collinear antiferromagnetic $FeGe_2$.

preferable candidate for the low-temperature ground-state phase of $FeGe_2$.

We next want to compare our results with available experimental data, discuss them, and check our conclusions about the low-temperature electronic and magnetic structures of iron digermanide.

4. The DHVA effect and related electronic properties

The de Haas–van Alphen effect has been observed in antiferromagnetic $FeGe_2$ [6, 8]

Table 2. The dependence of some physical quantities in non-collinear antiferromagnetic $FeGe_2$ on the angle 2φ between magnetic moment directions (per four molecules, Fe_4Ge_8; $a = 11.1$ au).

2φ	ΔE_{tot} (Ryd)	M (μ_B)	DOS(E_F) (states/(Ryd cell))
0°	- 0.2025	1.280	66.2
20°	- 0.2011	1.266	74.5
40°	- 0.1975	1.230	77.0
70°	- 0.1893	1.161	76.2

and revealed two closed sheets of the Fermi surface (FS) having comparatively small cyclotron masses. From the symmetry of the dependence of the DHVA frequencies it was concluded that these sheets have to be centred on the ΓZ line of the tetragonal Brillouin zone. None of these experimental data can be explained on the basis of the paramagnetic band structure [13] with its extremely flat energy bands near the Fermi energy.

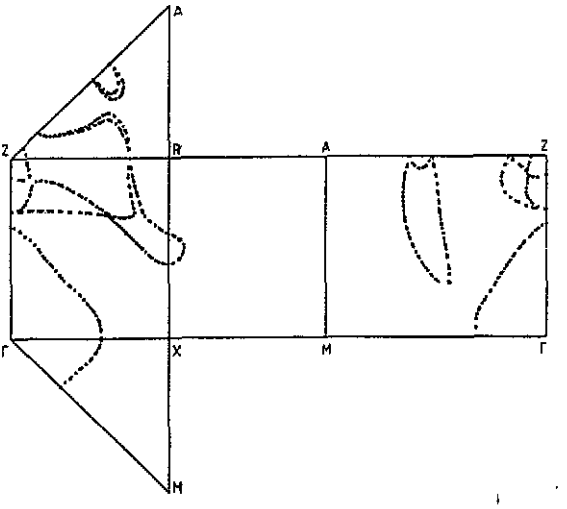

Figure 4. Fermi surface cross-sections for collinear antiferromagnetic $FeGe_2$.

Table 3. Comparison of measured and calculated de Haas–van Alphen data.

Direction of the magnetic field	S (10^{-2} Å^{-2})			m_c^* (au)		
	Experiment [6, 8]	Theory (collin.)	Theory (non-coll.)	Experiment [8]	Theory (collin.)	Theory (non-coll.)
[100]	19.3 ± 0.1	28.1	26.4	0.40 ± 0.01	0.24	0.5
[110]	17.1 ± 0.1	23.6	21.2	0.41 ± 0.01	0.27	0.57
[001]	15.1 ± 0.1	21.2	23.3	0.51 ± 0.02	0.33	0.37

The calculated collinear antiferromagnetic band-structure results in the Fermi surface cross-sections shown in figure 4. For the low-frequency DHVA signal the

identification of the corresponding FS sheet needs some additional experimental and theoretical effort. But the origin of the high-frequency DHVA signal seems rather evident and associated with the 'octahedron' centred at the Γ point. The calculated FS areas and cyclotron masses are listed in table 3 and can be compared with the experimental data. For the magnetic field directions considered the octahedron cross-sections have almost the same ratio as the experimental ones but are larger by $\simeq 30\%$ in absolute area. It needs only a shift by 7 mRyd of the calculated value of the Fermi energy to achieve a good fit with the experimental FS areas within the precision of experimental errors listed. The ratio of the experimental to calculated cyclotron masses for all three cross-sections varies between 1.5 to 1.6 giving reasonable values of the electron–phonon mass enhancement of $\lambda_{100} \simeq 0.6, \lambda_{110} \simeq 0.52$ and $\lambda_{001} \simeq 0.55$. From the low-temperature heat capacity data for $FeGe_2$ ($\gamma = 4.3$ mJ mol^{-1} K^{-2} [10]) together with our calculated value of the density of states at E_F the averaged value of $\lambda = 0.5$ appears to be in good agreement with the DHVA results.

For the proposed non-collinear antiferromagnetic model [2] with $2\varphi = 72°$ the calculations of FS cross-sections and cyclotron masses were carried out as well. In this case we still have an 'octahedron' at Γ but, as can be seen from table 3, with $S_{001} > S_{110}$. The last relation is not consistent with the experimental data [6, 8]. Moreover, for the non-collinear antiferromagnetic structure the electronic states on the main part of the 'octahedron' FS have pronounced d-like character giving a higher value of the density of states at E_F. So it seems not surprising that calculated cyclotron masses appear even larger than experimental ones for the orbits in the (100) and (110) planes.

We thus conclude that our calculations give strong support for the collinear antiferromagnetic structure of $FeGe_2$ at low temperatures giving the lowest total energy for this case. On the microscopic level the calculated FS cross-sections and cyclotron masses are in good agreement with the experimental data. Having not been able to study the anisotropy of the electron–phonon interaction, we nevertheless suggest the average value $\lambda \cong 0.5$ for $FeGe_2$ deduced from the DHVA and heat capacity data together with the results of band-structure calculations. For the alternative non-collinear model we obtained a higher value of the total energy and poor agreement with the DHVA experiment.

Acknowledgment

One of us (GEG) was supported by the DFG under SFB 252 Darmstadt, Frankfurt, Mainz (Federal Republic of Germany).

References

[1] Kren E and Szabo P 1964 *Phys. Lett.* **11** 215–6
[2] Forsyth J B, Johnson C E and Brown P J 1964 *Phil. Mag.* **10** 713–21
[3] Satya Murthy N S, Begum R J, Somanathan C S and Murphy M R L N 1965 *Solid State Commun.* **3** 113–6
[4] Solyom J and Kren E 1966 *Solid State Commun.* **4** 255–6
[5] Mikhel'son A V, Krentsis R P and Gel'd P V 1970 *Fiz. Tverd. Tela* **12** 2470–2 (Engl. Transl. 1971 *Sov. Phys.–Solid State* **12** 1979)
[6] Verkin B I, Pluzhnikov V B, Svechkarev I V, Fomenko Yu N, Geld P V and Krentsis R P 1978 *Inst. Phys. Conf. Ser.* **39** pp 617–9

[7] Dutchak Ya I, Kavich I V, Sinyushko V G, Shevchuk P I and Yatsyk B N 1979 *Ukr. Fiz. Zh.* **24** 1556–62
[8] Svechkarev I V, Fawcett E and Holroyd F W 1980 *Solid State Commun.* **35** 297-8
[9] Franus-Muir E, Fawcett E and Pluzhnikov V 1984 *Solid State Commun.* **52** 615–8
[10] Corliss L M, Hastings J M, Kunnmann W, Thomas R, Zhuang J, Butera R and Mukamel D 1985 *Phys. Rev.* B **31** 4337–46
[11] Venturini G, Fruchart D, Hubsch J, Le Caer G, Malaman B and Roques B 1985 *J. Phys. F: Met. Phys.* **15** 427–38
[12] Yasukochi K, Kanematsu K and Ohoyama T 1961 *J. Phys. Soc. Japan* **16** 429
[13] Skriver H L, Grechnev G E, Kruglov V O and Svechkarev I V 1987 *Fiz. Nizk. Temp.* **13** 765–8 (Engl. Transl. 1987 *Sov. J. Low. Temp. Phys.* **13** 438–9)
[14] Andersen O K 1975 *Phys. Rev.* B **12** 3060–83
[15] Skriver H L 1984 *The LMTO Method* (Berlin: Springer)
[16] Kübler J, Höck K-H, Sticht J and Williams A R 1988 *J. Phys. F: Met. Phys.* **18** 469–83
[17] Kübler J, Höck K-H, Sticht J and Williams A R 1988 *J. Appl. Phys.* **63** 3482–6
[18] Sticht J, Höck K-H and Kübler J 1989 *J. Phys.: Condens. Matter* **1** 8155–70
[19] Kohn W and Sham L J 1965 *Phys. Rev.* **140** A1133
von Barth U and Hedin L 1975 *J. Phys. C: Solid State Phys.* **5** 1629
[20] Williams A R, Kübler J and Gelatt C D Jr 1979 *Phys. Rev.* B **19** 6094–118